Liquid crystal phases of achiral banana-shaped molecules: a computer simulation study

R. Memmer

PLEASE SCROLL DOWN FOR ARTICLE

Liquid crystal phases of achiral banana-shaped molecules: a computer simulation study†

R. MEMMER

Fachbereich Chemie, Universität Kaiserslautern, D-67663 Kaiserslautern,
Germany; e-mail: memmer@rhrk.uni-kl.de

The phase behaviour of achiral banana-shaped molecules was studied by computer simulation. The banana-shaped molecules were described by model intermolecular interactions based on the Gay–Berne potential. The characteristic molecular structure was considered by joining two calamitic Gay–Berne particles through a bond to form a biaxial molecule of point symmetry group C_{2v} with a suitable bending angle. The dependence on temperature of systems of $N = 1024$ rigid banana-shaped molecules with bending angle $\varphi = 140°$ has been studied by means of Monte Carlo simulations in the isobaric–isothermal ensemble (NpT). On cooling an isotropic system, two phase transitions characterized by phase transition enthalpy, entropy and relative volume change have been observed. For the first time by computer simulation of a many-particle system of banana-shaped molecules, at low temperature an untilted smectic phase showing a global phase biaxiality and a spontaneous local polarization in the layers, i.e. a local polar arrangement of the steric dipoles, with an antiferroelectric-like superstructure could be proven, a phase structure which recently has been discovered experimentally. Additionally, at intermediate temperature a nematic-like phase has been proved, whereas close to the transition to the smectic phase hints of a spontaneous achiral symmetry breaking have been determined. Here, in the absence of a layered structure a helical superstructure has been formed. All phases have been characterized by visual representations of selected configurations, scalar and pseudoscalar correlation functions, and order parameters.

1. Introduction

A characteristic feature of many molecules forming thermotropic liquid crystal phases is their shape anisotropy; very often the corresponding molecules can be characterized as rod- or disk-shaped. Recently, new types of liquid crystal phases were discovered formed by so-called banana-shaped molecules [1]. Many of these phases show interesting material properties, e.g. the appearance of ferroelectricity which in liquid crystals was earlier mainly restricted to systems composed of chiral molecules [2]. In contrast, in polar liquid crystals of achiral banana-shaped molecules, the spontaneous polarization originates from a biaxial packing of their polar axes in smectic layers. Even more remarkable is the spontaneous achiral symmetry breaking, the formation of chiral superstructures by achiral molecules, in systems of banana-shaped molecules [3–8], a phenomenon well known, e.g. from crystallization processes, but not in

liquid crystals. Macroscopic chiral domains have been discovered in smectic phases of achiral banana-shaped molecules, whereas different phase structures are reported which consist of arrangements of chiral layers in antiferroelectric racemic or homogeneously chiral states [5]. Here, it should be pointed out that the chirality is not of molecular origin, but results from the combination of polar molecular orientational ordering around the layer normal and a molecular tilt. A challenging task currently under intensive investigation is the determination of structural properties of the multitude of liquid crystal phases formed by banana-shaped molecules and understanding their link to the molecular structure, in both cases especially with respect to the occurrence of spontaneous achiral symmetry breaking. Investigations by means of molecular modelling, e.g. Monte Carlo (MC) and molecular dynamics (MD) computer simulation, allow the deduction of such a link between microscopic and macroscopic properties starting with model interactions between the molecules, and have been successfully applied in the field of liquid crystals [9, 10]. Recently, a variety of model systems for biaxial molecules (defined as multiple-site models in order to describe

† Presented at the 18th International Liquid Crystal Conference, 24–28 July 2000, Sendai, Japan. This paper is dedicated to Professor Hans-Georg Kuball on the occasion of his 70th birthday.

the molecular structure of mesogenic molecules in more detail) have been studied by computer simulation, see e.g. [11–14]. In the following, a rigid banana-shaped Gay–Berne molecule of point symmetry group C_{2v} is defined by linking two Gay–Berne centres to take into account the characteristic features of banana-shaped molecules, especially a polar axis intersecting the bending angle. The phase structures of such achiral banana-shaped molecules will be investigated as a function of temperature by MC simulations under isobaric–isothermal conditions (NpT). The determination of the structural properties of the phases, focusing especially on a characterization of local phase biaxiality and polar order, will be of central interest.

2. Model system

A banana-shaped Gay–Berne molecule is defined by linking two equivalent calamitic Gay–Berne particles a and b to form an achiral molecule of point symmetry group C_{2v}. Whereas a typical banana-shaped molecule, figure 1(a), has an electric dipole along the polar axis intersecting the bending angle, the corresponding banana-shaped Gay–Berne molecule has a steric dipole only, figure 1(b), see e.g. [12–14]. The structure of the C_{2v}-symmetric banana-shaped molecule is defined by two internal coordinates: (i) the bending angle φ, which denotes the angle between the unit vectors $\hat{\mathbf{u}}_a$, $\hat{\mathbf{u}}_b$ along the particle symmetry axes, with possible values $0° < \varphi < 180°$; and (ii) the distance r_{ab}, which is the
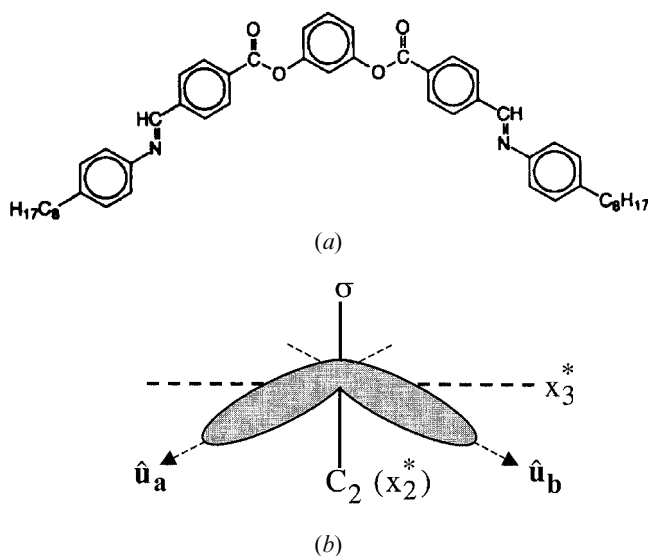

(a)

(b)

Figure 1. Banana-shaped molecules: (a) chemical structure of a typical banana-shaped molecule (figure from [1]); (b) a banana-shaped Gay–Berne molecule of point symmetry group C_{2v} with a steric dipole along the polar axis x_2^*, defined by linking two equivalent calamitic Gay–Berne particles.

absolute value of the intramolecular vector $\mathbf{r}_{ab} = \mathbf{r}_b - \mathbf{r}_a$ refering to the vectors $\mathbf{r}_a$ and $\mathbf{r}_b$ to the centres of the two Gay–Berne particles a and b. For this study a bending angle $\varphi = 140°$ has been chosen, a value in the typical range for banana-shaped molecules, see e.g. [15, 16]. A molecule-fixed coordinate system with axes x_i^* chosen parallel to selected symmetry-fixed axes is defined. x_3^* is taken parallel to the molecular long axis fixed by the intramolecular vector $\mathbf{r}_{ab}$, i.e. it corresponds to the normal of the mirror plane intersecting the bending angle. x_2^* has been taken along the polar axis intersecting the bending angle, i.e. parallel to the C_2 symmetry axis. Finally, x_1^* is defined perpendicular to both x_2^* and x_3^* in the way that a right-handed Cartesian coordinate system is obtained. The steric dipole $\boldsymbol{\mu}$ is fixed by symmetry along x_2^*. For convenience, $\boldsymbol{\mu}$ is chosen normalized to unity (i.e. $|\boldsymbol{\mu}| = 1$), and taken to point with its positive direction along the vector given by $\hat{\mathbf{u}}_a + \hat{\mathbf{u}}_b$.

The intermolecular interactions between two such molecules i and j separated by an intermolecular vector $\mathbf{R}_{ij} = 1/2[(\mathbf{r}_a^{(j)} + \mathbf{r}_b^{(j)}) - (\mathbf{r}_a^{(i)} + \mathbf{r}_b^{(i)})]$ with orientations denoted by Ω_i and Ω_j, respectively, where Ω comprises the Eulerian angles α, β, γ between the space-fixed x_i' ($i = 1, 2, 3$) coordinate system and the molecule-fixed x_i^* ($i = 1, 2, 3$) coordinate system of the corresponding molecule, are described by the sum of pair potentials between the Gay–Berne particles of the two molecules

$$U(\Omega_i, \Omega_j, \mathbf{R}_{ij}) = \sum_{\alpha = a,b} \sum_{\beta = a,b} U_a(\hat{\mathbf{u}}_\alpha^{(i)}, \hat{\mathbf{u}}_\beta^{(j)}, \mathbf{r}_{\alpha\beta}^{(i,j)}). \quad (1)$$

Here $\mathbf{r}_{\alpha\beta}^{(i,j)} = \mathbf{r}_\beta^{(j)} - \mathbf{r}_\alpha^{(i)}$ denotes the intermolecular vector between the centre of part α of molecule i and the centre of part β of molecule j with $\alpha, \beta = a, b$. The interaction potential U_a between the parts of molecules i and j is the Gay–Berne potential [17], which includes the molecular anisotropy in both the shape and the attractive forces and has been successfully used to describe, for example, calamitic liquid crystals [18]:

$$U_a(\hat{\mathbf{u}}_\alpha^{(i)}, \hat{\mathbf{u}}_\beta^{(j)}, \mathbf{r}_{\alpha\beta}^{(i,j)})$$

$$= 4\varepsilon(\hat{\mathbf{u}}_\alpha^{(i)}, \hat{\mathbf{u}}_\beta^{(j)}, \hat{\mathbf{r}}_{\alpha\beta}^{(i,j)}) \left\{ \left(\frac{\sigma_0}{r_{\alpha\beta}^{(i,j)} - \sigma(\hat{\mathbf{u}}_\alpha^{(i)}, \hat{\mathbf{u}}_\beta^{(j)}, \hat{\mathbf{r}}_{\alpha\beta}^{(i,j)}) + \sigma_0} \right)^{12} \right.$$

$$\left. - \left(\frac{\sigma_0}{r_{\alpha\beta}^{(i,j)} - \sigma(\hat{\mathbf{u}}_\alpha^{(i)}, \hat{\mathbf{u}}_\beta^{(j)}, \hat{\mathbf{r}}_{\alpha\beta}^{(i,j)}) + \sigma_0} \right)^{6} \right\} \quad (2)$$

where $\hat{\mathbf{r}}_{\alpha\beta}^{(i,j)}$ denotes the unit vector parallel to $\mathbf{r}_{\alpha\beta}^{(i,j)}$ and $r_{\alpha\beta}^{(i,j)} = |\mathbf{r}_{\alpha\beta}^{(i,j)}|$. The explicit expressions for the orientation-dependent parameters $\sigma(\hat{\mathbf{u}}_\alpha^{(i)}, \hat{\mathbf{u}}_\beta^{(j)}, \hat{\mathbf{r}}_{\alpha\beta}^{(i,j)})$ and $\varepsilon(\hat{\mathbf{u}}_\alpha^{(i)}, \hat{\mathbf{u}}_\beta^{(j)}, \hat{\mathbf{r}}_{\alpha\beta}^{(i,j)})$ are given in [18].

It should be pointed out that no dipolar interaction term is taken into account. The polar axis of the molecule exists due to steric reasons only, introduced here on a molecular level by the relative orientation of the two

calamitic parts of each molecule defining a bending angle. In the following, neglecting internal degrees of freedom, the molecules are considered as rigid objects. All intramolecular interactions of rigid banana-shaped Gay–Berne molecules are given by additive constants which have been omitted for convenience, and all parameters of the Gay–Berne potential which define in detail the molecular properties are treated as temperature and pressure independent.

3. Computational details

For the banana-shaped Gay–Berne molecules, treated as rigid during the simulation, a bending angle of $\varphi = 140°$ has been chosen, a value in the typical range of banana-shaped molecules [15, 16]. The distance r_{ab} has been chosen related to the bending angle according to $r_{ab} = [2(1 - \cos \varphi)]^{1/2}$ which yields $r_{ab} \approx 1.88$; i.e. a considerable overlap of the two Gay–Berne particles in the central part of the molecule has been taken into account. For the Gay–Berne particles a parameterization was used with parameter values $\sigma_e/\sigma_s = 3$, $\varepsilon_e/\varepsilon_s = 0.2$, $\mu = 1$ and $v = 2$, necessary for the determination of the functions $\sigma(\hat{\mathbf{u}}_\alpha^{(i)}, \hat{\mathbf{u}}_\beta^{(j)}, \hat{\mathbf{r}}_{\alpha\beta}^{(i,j)})$ and $\varepsilon(\hat{\mathbf{u}}_\alpha^{(i)}, \hat{\mathbf{u}}_\beta^{(j)}, \hat{\mathbf{r}}_{\alpha\beta}^{(i,j)})$, which has already been studied for the calamitic Gay–Berne fluid [18].

Systems composed of such achiral banana-shaped Gay–Berne molecules were studied in a rectangular box at constant number of particles N, pressure p and temperature T, i.e. in the isobaric–isothermal ensemble (NpT), using the standard Metropolis Monte Carlo technique [19]. Periodic boundary conditions and nearest image summation were applied. Dimensionless units are used in the following: scaled temperature $T^* = k_B T/\varepsilon_0$, scaled pressure $p^* = p\sigma_0^3/\varepsilon_0$, scaled internal energy per molecule $\langle U^* \rangle = \langle U \rangle/\varepsilon_0$, scaled enthalpy per molecule $\langle H^* \rangle = \langle H \rangle/\varepsilon_0$, scaled box length $L_i^* = L_i/\sigma_0$ with $i = x, y, z$, scaled volume per molecule $\langle V^* \rangle = \langle V \rangle/(N\sigma_0^3)$ with $\langle V \rangle = \langle L_x L_y L_z \rangle$, and scaled distance $r^* = |\mathbf{R}_{ij}|/\sigma_0$. All simulations were done at a pressure $p^* = 3$, i.e. under similar conditions under which in a recent study of Gay–Berne systems a rich polymorphism has been observed [20], applying a spherical cut-off at the selected distance $r_{\alpha\beta}^{(i,j)}/\sigma_0 = 3.8$. A trial configuration was generated by a random translation of the chosen molecule followed by a random rotation about one of the randomly chosen space-fixed axes. The maximum rotation was fixed to 2.5°, the maximum displacement of the molecules was adjusted during the simulation to achieve an acceptance ratio of 1/2. A cycle consists of N such canonical moves followed by an attempt to modify the volume, where a box edge was selected at random and the logarithm of its length was changed randomly. In order to decide whether such a move should be accepted or not, the corresponding acceptance rule acc$(o \rightarrow n) = \min(1, \exp[-\beta(\Delta U + p\Delta V) - (N + 1)\Delta \ln V])$ has been

applied [19]. Here, Δ denotes the difference in the corresponding quantity before and after the attempted move, i.e. in the old (o) and new (n) configurations, respectively. The maximum displacement in $\ln L_i^*$ has been adjusted during the simulation to achieve an acceptance ratio of 1/2.

The starting configurations for the NpT simulations were created by MC simulations in the NVT ensemble under periodic boundary conditions where initial configurations with randomly distributed molecular positions and orientations were used. Systems with $N = 1024$ banana-shaped molecules were equilibrated at $V^* = 3.\bar{3}$ and $T^* = 3$ in a cubic simulation box of corresponding length L^*. Two independent simulation runs were performed, and each time an isotropic phase was obtained. A configuration of the isotropic phase was used as initial configuration for the corresponding NpT simulation. The thermodynamic properties were studied in two independent simulation runs as a function of the temperature T^*, cooling with a step size of $\Delta T^* = -0.25$ along the selected isobar. Final configurations obtained for nearby values of T^* were taken as the initial configuration for the subsequent run. For each state point, generally an equilibration run of 800 kc (1 kc denotes 1000 cycles) was followed by a production run of 200 kc. All thermodynamic properties of interest were calculated every ten cycles and averaged over the production run. Additionally, correlation functions were calculated from data taken after every tenth cycle of a subsequent 10 kc production run.

4. Order parameters and correlation functions

In order to characterize the long-range orientational order of the biaxial molecules, second rank order parameters $\langle P_2 \rangle^{(i)}$, where $i = 1, 2, 3$ refers to the corresponding molecule-fixed x_i^* axis, were calculated during the production runs. They are given by the largest eigenvalue of the corresponding tensor

$$S_{\alpha\beta}^{(i)} = \frac{1}{N} \sum_{j=1}^{N} \left[\frac{3}{2} \hat{x}_{j\alpha}^{(i)} \hat{x}_{j\beta}^{(i)} - \frac{1}{2} \delta_{\alpha\beta} \right], \quad (3)$$

where $\alpha, \beta = x, y, z$ and $\hat{x}_j^{(i)}$ denotes a unit vector along the molecule-fixed x_i^* axis ($i = 1, 2, 3$) of a molecule j, i.e.

$$\langle P_2 \rangle^{(i)} = \left\langle \frac{1}{2} (3 \cos^2 \beta_j^{(i)} - 1) \right\rangle. \quad (4)$$

Here, $\beta_j^{(i)}$ denotes the angle between the molecule-fixed x_i^* axis of a molecule j and the corresponding director $\hat{\mathbf{n}}_i$ given by the eigenvector corresponding to the largest eigenvalue, i.e. $\langle P_2 \rangle^{(i)}$ is equal to the Saupe order parameter calculated for the corresponding molecule-fixed axis x_i^*.

Additionally, for a description of the local order in a phase with a helical superstructure along a selected space-fixed direction, the corresponding local order parameter $\langle \tilde{P}_2 \rangle^{(3)}$ has been calculated, as introduced in [11]. The superscript ~ denotes the reference of the local order parameter to a local space-fixed axis defined parallel to the local director $\hat{\mathbf{n}}(z)$ of the helical phase given by

$$\hat{\mathbf{n}}(z) = \begin{pmatrix} \sin\theta\cos\varphi z \\ \sin\theta\sin\varphi z \\ \cos\theta \end{pmatrix} \qquad (5)$$

i.e. the local director $\hat{\mathbf{n}}(z)$ is assumed to be tilted at a constant tilt angle θ to the helical axis $\hat{\mathbf{p}}$ and continuously spiraling around $\hat{\mathbf{p}}$, chosen parallel to z, according to the periodicity given through the pitch P defining the azimuthal angle via $\varphi = 2\pi/P$. For example, an angle of $\theta = 90°$ corresponds to the situation in a cholesteric phase with local director $\hat{\mathbf{n}}(z)$ always perpendicular to $\hat{\mathbf{p}}$. Under the assumption of a local orientational distribution function which is independent of z, the local order parameter can be calculated as introduced in [11], mapping each configuration of the helical phase back to a nematic phase by a corresponding transformation around z, followed by the diagonalization of the $\tilde{S}_{\alpha\beta}^{(3)}$ tensor defined analogously to $S_{\alpha\beta}^{(3)}$. Then, the tilt angle θ is given by the angle between the z axis and the eigenvector corresponding to the largest eigenvalue of $\tilde{S}_{\alpha\beta}^{(3)}$. Therefore, the local order parameter

$$\langle \tilde{P}_2 \rangle^{(3)} = \left\langle \frac{1}{2}(3\cos^2\tilde{\beta}_j^{(3)} - 1) \right\rangle \qquad (6)$$

describes the distribution of the molecule-fixed x_3^* axes with respect to the local director $\hat{\mathbf{n}}(z)$, whereas $\tilde{\beta}_j^{(3)}$ denotes the angle between the molecule-fixed x_i^* axis of a molecule j and the corresponding local director $\hat{\mathbf{n}}(z)$.

In order to characterize the structural properties of the phases, more detailed averages of a suitable subset of the rotational invariant functions $S_{l_1 l_2 m}^{(\alpha,\beta)}(\hat{\mathbf{x}}_i^{(\alpha)}, \hat{\mathbf{x}}_j^{(\beta)}, \hat{\mathbf{r}}_{ij})$ introduced by Stone [21] were considered, where $\hat{\mathbf{x}}_i^{(\alpha)}$ denotes a unit vector along the molecule-fixed x_α^* axis ($\alpha = 1, 2, 3$) of a molecule i and $\hat{\mathbf{r}}_{ij}$ the unit vector along the intermolecular separation vector $\mathbf{R}_{ij}$ between molecules i and j. The radial orientational correlation functions, calculated in spherical shells around a molecule, i.e. as a function of the intermolecular separation r^*, are denoted by

$$S_{l_1 l_2 m}^{(\alpha,\beta)}(r^*) = \langle S_{l_1 l_2 m}^{(\alpha,\beta)}(\hat{\mathbf{x}}_i^{(\alpha)}, \hat{\mathbf{x}}_j^{(\beta)}, \hat{\mathbf{r}}_{ij}) \rangle_{(r^*)_{ij}} \qquad (7)$$

where the subscript $(r^*)_{ij}$ denotes the average over all pairs of molecules of a configuration separated by a distance r^*.

Explicitly, the scalar (even 'total rank' $l_1 + l_2 + m$) radial orientational correlation function

$$S_{220}^{(3,3)}(r^*) = \frac{1}{2\sqrt{5}} \langle 3(\hat{\mathbf{x}}_i^{(3)} \cdot \hat{\mathbf{x}}_j^{(3)})^2 - 1 \rangle_{(r^*)_{ij}} \qquad (8)$$

was calculated.

Additionally, corresponding longitudinal orientational correlation functions

$$S_{l_1 l_2 m}^{(\alpha,\beta)}(r_\parallel^*) = \langle S_{l_1 l_2 m}^{(\alpha,\beta)}(\hat{\mathbf{x}}_i^{(\alpha)}, \hat{\mathbf{x}}_j^{(\beta)}, \hat{\mathbf{r}}_\parallel) \rangle_{(r_\parallel^*)_{ij}} \qquad (9)$$

were considered, defined as a function of the intermolecular separation $r_\parallel^*$ along a suitably chosen space-fixed reference axis $\mathbf{r}_\parallel$ with unit vector $\hat{\mathbf{r}}_\parallel$. The subscript $(r_\parallel^*)_{ij}$ denotes the average over pairs of molecules of a configuration separated by a distance $r_\parallel^*$ along the reference axis.

Explicitly, in order to characterize the polar order, the polar orientational correlation function

$$S_{110}^{(2,2)}(r_\parallel^*) = -\frac{1}{\sqrt{3}} \langle (\hat{\mathbf{x}}_i^{(2)} \cdot \hat{\mathbf{x}}_j^{(2)}) \rangle_{(r_\parallel^*)_{ij}} \qquad (10)$$

was calculated. Additionally, in order to characterize helical superstructures, the pseudoscalar (odd 'total rank' $l_1 + l_2 + m$) radial orientational correlation function

$$S_{221}^{(3,3)}(r^*) = -\sqrt{\frac{3}{10}} \langle [(\hat{\mathbf{x}}_i^{(3)} \times \hat{\mathbf{x}}_j^{(3)}) \cdot \hat{\mathbf{r}}_{ij}](\hat{\mathbf{x}}_i^{(3)} \cdot \hat{\mathbf{x}}_j^{(3)}) \rangle_{(r^*)_{ij}}$$

$$\qquad (11)$$

was calculated.

In order to characterize the positional order, several pair distribution functions independent of the molecular orientations $\hat{\mathbf{x}}_i^{(\alpha)}$ ($\alpha = 1, 2, 3$) and the intermolecular vector $\hat{\mathbf{r}}_{ij}$, have been calculated. The radial distribution function $S_{000}(r^*)$ describes the distribution of particle centres as a function of the molecular separation r^*. The longitudinal distribution function $S_{000}(r_\parallel^*)$ characterizes the distribution of particle centres as a function of the intermolecular separation $r_\parallel^*$ along a space-fixed reference axis $\mathbf{r}_\parallel$, and the transversal distribution function $S_{000}(r_\perp^*)$ as a function of the intermolecular separation $r_\perp^*$ perpendicular to a space-fixed reference axis $\mathbf{r}_\parallel$.

5. Results and discussion

The phase properties of systems composed of banana-shaped molecules were studied as a function of temperature along an isobar. At the highest temperature studied, $T^* = 3$, an isotropic phase is stable; the corresponding characteristics are apparent from the snapshot of the configuration shown in figure 2. In order to have a schematic representation of its general shape, each banana-shaped molecule is represented by a rotationally symmetric ellipsoid for each of its Gay–Berne particles with an axis ratio of $1:1:3$ corresponding to the parameter
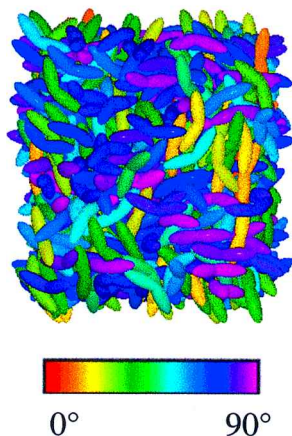
Figure 2. Snapshot of the molecular organization in the isotropic phase formed at $T^* = 3$. Each banana-shaped molecule is represented by an ellipsoid for each of its two Gay–Berne particles which are colour-coded with respect to the angle between its molecular long axis x_3^* and the vertically oriented box normal.

value $\sigma_e/\sigma_s = 3$ and colour-coded with respect to the angle between its molecular long axis x_3^* and a selected box normal.

In the following, the different phases and phase transitions will be characterized, leading to an identification of the phase sequence isotropic, nematic, and smectic with decreasing temperature. The thermodynamic properties, which have been obtained in good agreement from two independent cooling sequences, are shown in figure 3 as functions of temperature. The scaled volume per molecule $\langle V^* \rangle$, figure 3 (a), shows a small but significant jump in the temperature range $2.25 \leqslant T_{tr}^* \leqslant 2.50$ indicating a weak first order phase transition from the isotropic phase to a phase which will be identified as nematic later in this section. A second phase transition connected with a comparable large change in $\langle V^* \rangle$, i.e. an increased strength of the transition, is obvious in the temperature range $1.50 \leqslant T_{tr}^* \leqslant 1.75$ to a phase identified later as smectic. Both phase transitions are further confirmed by discontinuities in identical temperature regions of the scaled enthalpy per molecule $\langle H^* \rangle$, figure 3 (b), which has been calculated according to $\langle H^* \rangle = \langle U^* \rangle + p^* \langle V^* \rangle$.

In order to characterize the nature of the phase transitions, several thermodynamic quantities have been determined following Hashim *et al.* [22]. At the transition assumed at temperature $T^* = 2.375$, i.e. midway between the lowest temperature $T^* = 2.50$ in the isotropic phase and the highest temperature $T^* = 2.25$ in the nematic phase, a relative change of 2.2% in volume at the transition $\Delta V^*/V^*$ was estimated according to

$$\Delta V^*/V^* = 2(\langle V_I^* \rangle - \langle V_N^* \rangle)/(\langle V_I^* \rangle + \langle V_N^* \rangle) \quad (12)$$

from extrapolated values for $\langle V_I^* \rangle$ and $\langle V_N^* \rangle$ assuming linear dependences of the corresponding volumes on
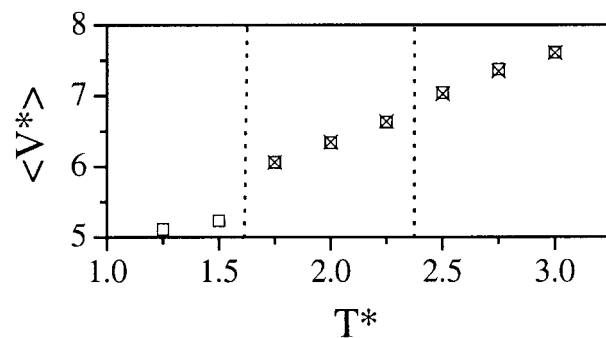
(a)
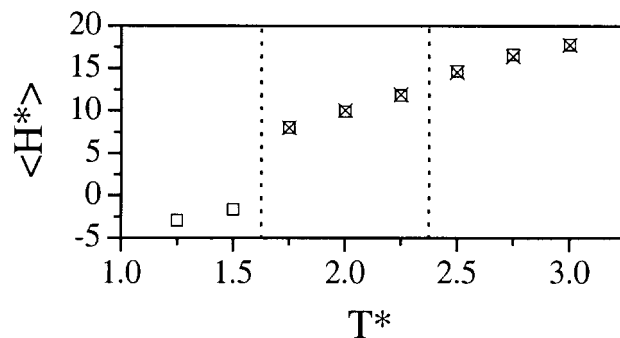
(b)

Figure 3. Dependence of thermodynamic properties on scaled temperature T^*: (a) scaled volume per molecule $\langle V^* \rangle$; (b) scaled enthalpy per molecule $\langle H^* \rangle$. Results are shown from two independent cooling sequences ($\square$, $\times$); dashed vertical lines indicate the phase transition regions.

temperature. Analogously, a relative change of 11.2% in volume at the transition was calculated for the phase transition from the nematic phase to the smectic phase at $T^* = 1.625$. Extrapolating the enthalpies in the corresponding phases to the transition temperature, assuming a linear temperature dependence, yields phase transition enthalpies $\Delta H^* = 1.18$ at $T^* = 2.375$ and $\Delta H^* = 8.08$ at $T^* = 1.625$, respectively. The relation $\Delta S/R = \Delta H^*/T^*$ yields the corresponding phase transition entropies, $\Delta S/R = 0.49$ at $T^* = 2.375$ and $\Delta S/R = 4.97$ at $T^* = 1.625$. All calculated values are summarized in the table which includes for comparison corresponding values for phase transitions in the achiral calamitic Gay–Berne fluid [22, 23]. The values for $\Delta V^*/V^*$, ΔH^* and $\Delta S/R$ at the phase transition at $T^* = 2.375$ are much smaller than the corresponding values at the phase transition at $T^* = 1.625$. All thermodynamic quantities calculated at the high temperature phase transition are comparable in size to those determined at an N–I transition in the achiral calamitic Gay–Berne fluid, whereas at the low temperature phase transition they are of similar size or even higher compared with the corresponding values

Table.   Thermodynamic quantities characterizing selected phase transitions observed in Gay–Berne systems studied by isobaric–isothermal Monte Carlo simulations: relative change in volume at transition $\Delta V^*/V^*$, transition enthalpy ΔH^* and transition entropy $\Delta S/R$.

Transition	p^*	T^*	$\Delta V^*/V^*/\%$	ΔH^*	$\Delta S/R$	Ref.
N–I	3	2.375	2.2	1.18	0.49	this work
C_{PA}–N[a]	3	1.625	11.2	8.08	4.97	this work
SmB–I	1	0.625	14.0	2.23	3.57	[22]
N–I	2	1.675	4.2	0.80	0.47	[23]

[a] C_{PA} is an orthogonal biaxial smectic phase with antiferroelectric polar order.

determined at a SmB–I phase transition, emphasizing that here a highly ordered phase must be involved. Due to the small number of examples of banana-shaped molecules which exhibit a nematic phase, see for example [24, 25], only a very limited comparison with experimentally determined values is possible. The first example showing a nematic phase intermediate between the isotropic and a smectic is given by a $2'$-nitro-substituted m-terphenyl derivative [24]. Here, at the Sm–N transition the phase transition enthalpy is about twenty times larger than the corresponding quantity at the N–I transition, whereas in the simulation it is only about ten times larger.

In order to obtain a first insight into the structural changes connected with the appearing phase transitions, the order parameters $\langle P_2 \rangle^{(i)}$ ($i = 1, 2, 3$) have been calculated. Shown in figure 4 is the evolution of the order parameters $\langle P_2 \rangle^{(2)}$ and $\langle P_2 \rangle^{(3)}$ during the simulation at two selected temperatures close to phase transitions, which document the spontaneous formation of ordered systems. At $T^* = 2.25$, figure 4(a), the order parameter $\langle P_2 \rangle^{(3)}$, calculated with respect to a space-fixed axis which defines the director $\hat{\mathbf{n}}_3$, increases from values close to zero up to about $\langle P_2 \rangle^{(3)} \approx 0.6$. The molecules are aligned with their molecule-fixed x_3^* axes preferred parallel to each other; this behaviour indicates a phase transition from a disordered to an ordered phase which is consistent with a transition from an isotropic to a nematic phase. In contrast, the order parameters $\langle P_2 \rangle^{(2)}$, shown in figure 4(a), as well as $\langle P_2 \rangle^{(1)}$ remain close to zero; i.e. there exists no long range orientational order with respect to the molecule-fixed x_1^* and x_2^* axes. At $T^* = 1.50$, figure 4(b), the order parameters show a different behaviour: there is an obvious significant jump of the order parameter $\langle P_2 \rangle^{(3)}$ up to values of about $\langle P_2 \rangle^{(3)} \approx 0.98$; additionally there exists long range orientational order with respect to the molecule-fixed x_1^* and x_2^* axes. A biaxial phase has been formed expressed by values of the order parameter $\langle P_2 \rangle^{(2)} \approx 0.7$, which have been calculated with respect to director $\hat{\mathbf{n}}_2$ found to be perpendicular to $\hat{\mathbf{n}}_3$.

The average values of the order parameters $\langle P_2 \rangle^{(2)}$ and $\langle P_2 \rangle^{(3)}$ are shown as functions of temperature in
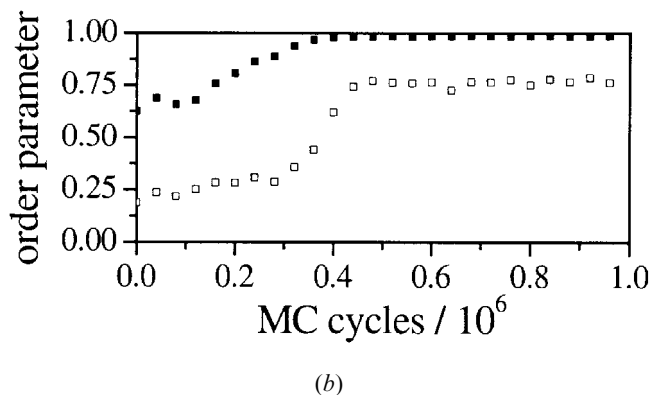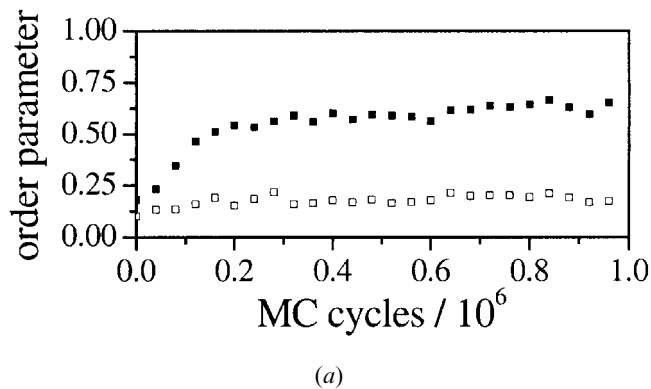

(a)

(b)

Figure 4.   Evolution of the order parameters $\langle P_2 \rangle^{(2)}$ ($\square$) and $\langle P_2 \rangle^{(3)}$ ($\blacksquare$) during the simulation run: (a) at $T^* = 2.25$; (b) at $T^* = 1.50$.

figure 5, and three different phase regions are obvious. In the temperature range of the isotropic phase, from $T^* = 2.5$ to $T^* = 3.0$, both order parameters are close to zero. At $T^* = 2.5$, close to the phase transition, $\langle P_2 \rangle^{(3)}$ starts increasing. In the temperature region from $T^* = 1.75$ to 2.25, a nematic-like phase has been formed with order parameters $\langle P_2 \rangle^{(3)}$ characterizing the order of the molecular long axes x_3^* with respect to the director $\hat{\mathbf{n}}_3$. With decreasing temperature $\langle P_2 \rangle^{(3)}$ remains comparably small, compared for example with the typical behaviour in nematic phases of the uniaxial Gay–Berne fluid [26]. The existing long range orientational order
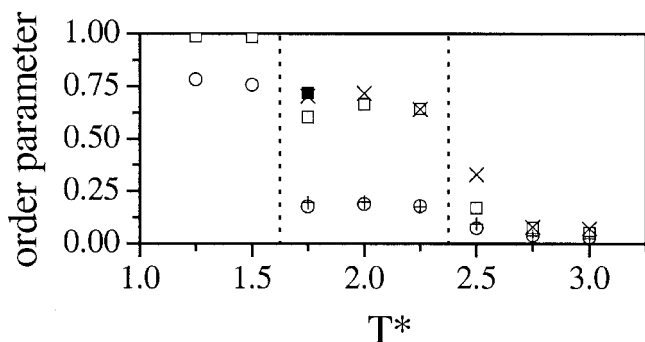
Figure 5. Dependence of the order parameters on the scaled temperature T^*: $\langle P_2 \rangle^{(2)}$ ($\bigcirc$), $\langle P_2 \rangle^{(3)}$ ($\square$). Additionally shown are results from a second independent cooling sequence ($+$, $\times$), and the local order parameter $\langle \check{P}_2 \rangle^{(3)}$ calculated at $T^* = 1.75$ with respect to a spiralling local director $\hat{n}(z)$ ($\blacksquare$). Dashed vertical lines indicate the phase transition regions.

of the x_3^* axes, which are defined perpendicular to x_2^*, leads to a limiting value $\langle P_2 \rangle^{(2)}_{\min}$ above zero, i.e. the small non-zero values of $\langle P_2 \rangle^{(2)}$ obtained here do not express a long range orientational order of the x_2^* axes. In contrast, after the second phase transition the values of $\langle P_2 \rangle^{(2)}$ are significantly above the limiting value $\langle P_2 \rangle^{(2)}_{\min} = 0.25$ in a system with orientations randomly distributed in a plane, i.e. considering $\langle P_2 \rangle^{(3)} = 1$ which is close to the obtained $\langle P_2 \rangle^{(3)}$ values. This clearly documents the spontaneous formation of a biaxial phase whereas $\langle P_2 \rangle^{(2)}$ slightly increases with decreasing temperature. In the biaxial phase there exists, as well as a long range orientational order of the x_3^* axes with respect to director $\hat{n}_3$, a long range orientational order of the x_2^* axes with respect to director $\hat{n}_2$ found to be perpendicular to $\hat{n}_3$. Shown in figure 5 are also results from a second independent cooling run, which confirm the formation of the nematic phase. In spite of the good agreement of the thermodynamic properties $\langle V^* \rangle$ and $\langle H^* \rangle$ obtained from both simulation runs (figure 3), there are significant differences with respect to the order parameter $\langle P_2 \rangle^{(3)}$ close to the second phase transition, where in one simulation run a phase with a comparable low order parameter was obtained, a feature which will be discussed in detail later.

In agreement with the chosen phase assignments are the structural properties which will be analysed considering selected correlation functions. Shown in figure 6 are the radial distribution function $S_{000}(r^*)$, which characterizes the distribution of the particle centres as a function of the intermolecular separation r^*, and the scalar radial orientational pair correlation function of rank two $S_{220}^{(3,3)}(r^*)$, giving insight into the orientational order with respect to the molecule-fixed x_3^* axes. In the shown temperature range from $T^* = 3.00$ to $T^* = 1.75$, short range positional order exists which is enlarged
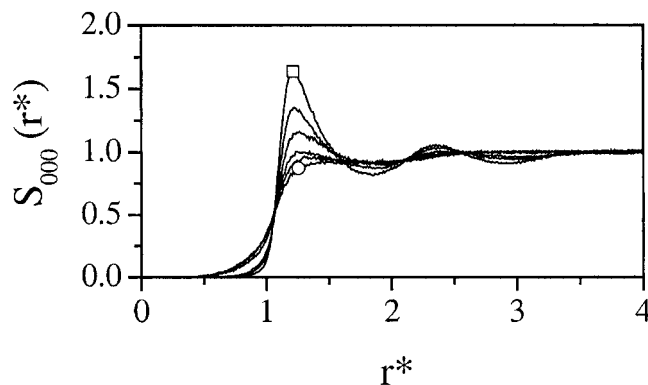
(a)
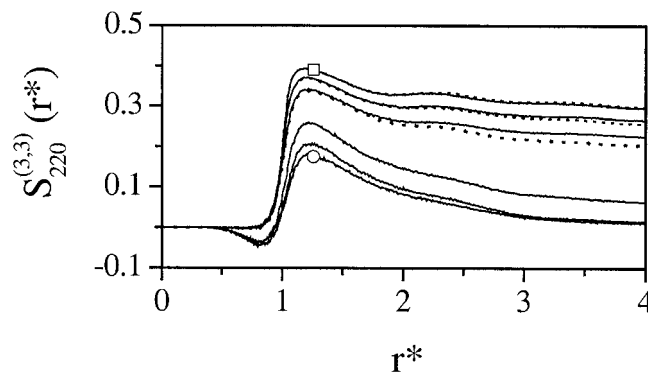
(b)

Figure 6. Correlation functions as a function of the intermolecular separation r^* at temperatures T^* in the temperature range from $T^* = 3.00$ ($\bigcirc$) to $T^* = 1.75$ ($\square$): (a) radial distribution function $S_{000}(r^*)$; (b) scalar radial orientational pair correlation function of rank two $S_{220}^{(3,3)}(r^*)$.

with decreasing temperature, but the lack of long range structure of $S_{000}(r^*)$, e.g. for separations $r^* > 3.5$, figure 6(a), indicates an isotropic distribution of the molecular centres consistent with the characteristics of isotropic and nematic phases. Independent of temperature, $S_{220}^{(3,3)}(r^*)$, figure 6(b), shows a positive maximum at short distances, i.e. the existence of a preferred parallel orientation of the x_3^* axes of neighbouring molecules, which is more extended at lower temperatures. In the temperature range of the isotropic phase, $S_{220}^{(3,3)}(r^*)$ rapidly tends to zero, i.e. there exists no long range orientational order. At these high temperatures, there even appear molecules separated by short distances below $r^* = 1$ as obvious from $S_{000}(r^*)$. The corresponding negative values of $S_{220}^{(3,3)}(r^*)$ at these distances document the formation of dimers of banana-shaped molecules with the x_3^* axis preferred perpendicular to each other, a feature which completely disappears on cooling. In a recent study of banana-shaped molecules

composed of two hard spherocylinders for selected bending angles, such an interlocking of pairs of banana-shaped molecules even excluded any spontaneous orientational ordering [13]. Remarkable is the long range behaviour of $S_{220}^{(3,3)}(r^*)$ at lower temperatures. The functions $S_{220}^{(3,3)}(r^*)$ at all temperatures in the range from $T^* = 2.25$ to $T^* = 1.75$ are significantly non-zero for all distances. $S_{220}^{(3,3)}(r^*)$ decreases with increasing intermolecular separation, but even for the largest separation considered, $S_{220}^{(3,3)}(r^*)$ does not reach a plateau value as expected in a nematic phase, a feature which could be due to the comparatively small system size studied.

At the second phase transition, significant changes appear with respect to the positional order, as is obvious on considering the radial distribution function $S_{000}(r^*)$ and the longitudinal distribution function $S_{000}(r_\parallel^*)$ calculated as functions of the intermolecular separation $r_\parallel^*$ along director $\hat{\mathbf{n}}_3$. At $T^* = 1.50$ the features of $S_{000}(r^*)$ up to the largest separations document the existence of long range positional order, figure 7(a). In contrast to

the behaviour of $S_{000}(r_\parallel^*)$ at $T^* = 1.75$, here the function is close to unity for all distances $r_\parallel^*$, documenting a uniform density distribution along director $\hat{\mathbf{n}}_3$, there exists at $T^* = 1.50$ a significant long range positional order along $\hat{\mathbf{n}}_3$ which is obvious from the periodic modulations, figure 7(b). A layered phase has been formed with an approximate layer distance of $d_0^* \approx 4.42$ estimated from the separation between the maxima of $S_{000}(r_\parallel^*)$. In order to determine correlations between the positions of molecules in different layers, the corresponding transversal distribution function $S_{000}(r_\perp^*)$ is given in figure 7(a) showing its dependence on the intermolecular separation $r_\perp^*$ perpendicular to director $\hat{\mathbf{n}}_3$. It shows comparable small features only, which are mainly related to contributions from molecules of the same layer, i.e. the phase is a smectic rather than a crystal phase. In order to determine whether a tilted or untilted layered phase was formed, the layer normal $\hat{l}$ has been calculated similarly to the procedure described in [27]. First, for each molecule i a local layer normal $\hat{\mathbf{l}}_i$ has been determined as eigenvector to the largest eigenvalue of the tensor

$$Q_{\alpha\beta}^i = \frac{1}{n(n-1)} \sum_{j=1}^{n} \sum_{k}^{n} \left[\frac{3}{2} (\hat{\mathbf{r}}_{ij} \times \hat{\mathbf{r}}_{ik})_\alpha (\hat{\mathbf{r}}_{ij} \times \hat{\mathbf{r}}_{ik})_\beta - \frac{1}{2} \delta_{\alpha\beta} \right] \tag{13}$$

where $\hat{\mathbf{r}}_{ij}$ is the unit vector between molecule i and one of its $n = 6$ nearest neighbours; then the tensor

$$Q_{\alpha\beta} = \frac{1}{N} \sum_{i=1}^{N} \left[\frac{3}{2} \hat{\mathbf{l}}_{i\alpha} \hat{\mathbf{l}}_{i\beta} - \frac{1}{2} \delta_{\alpha\beta} \right] \tag{14}$$

has been constructed, which after diagonalization yields the layer normal $\hat{\mathbf{I}}$ as eigenvector to the largest eigenvalue. In all configurations analysed the tilt angle, defined as the angle between the layer normal $\hat{\mathbf{I}}$ and the director $\hat{\mathbf{n}}_3$, was always below $2°$, i.e. insignificantly small. An untilted layered phase has been formed with the molecular long axes x_3^* of the banana-shaped molecules oriented preferred parallel to a director $\hat{\mathbf{n}}_3$ along the layer normal $\hat{\mathbf{I}}$.

This dramatic change of the structural properties is evident from the snapshot shown in figure 8 where a configuration selected from the production run at $T^* = 1.50$ is presented. Shown in figure 8(a) is the configuration with vertically aligned layer normal $\hat{\mathbf{I}}$ where each banana-shaped molecule is represented by spheres for its two Gay–Berne centres. A phase with non-interdigitated layers and a well defined layer distance d_0^* has been formed in a cooling sequence starting from a configuration with molecules randomly distributed in a cubic simulation box, while it should be mentioned that at no time has an external orienting field been applied in order to favour such a behaviour. Inside the simulation
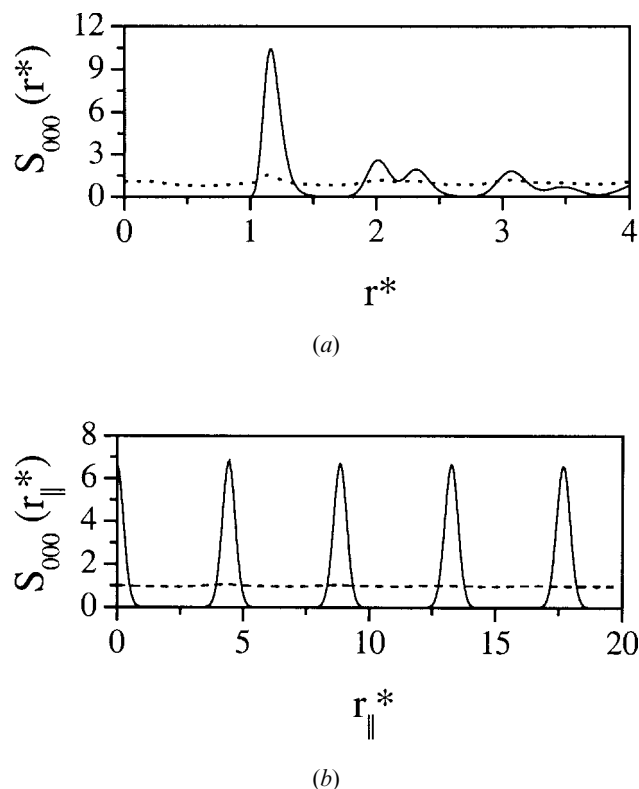
Figure 7. Correlation functions at temperature $T^* = 1.50$: (a) radial distribution function $S_{000}(r^*)$ and its dependence on the intermolecular separation r^* (—), additionally shown is the transversal distribution function $S_{000}(r_\perp^*)$ and its dependence on the intermolecular separation $r_\perp^*$ perpendicular to director $\hat{\mathbf{n}}_3$, (- - -); (b) longitudinal distribution function $S_{000}(r_\parallel^*)$ and its dependence on the intermolecular separation $r_\parallel^*$ along director $\hat{\mathbf{n}}_3$ (—), additionally shown is $S_{000}(r_\parallel^*)$ at temperature $T^* = 1.75$ (- -).
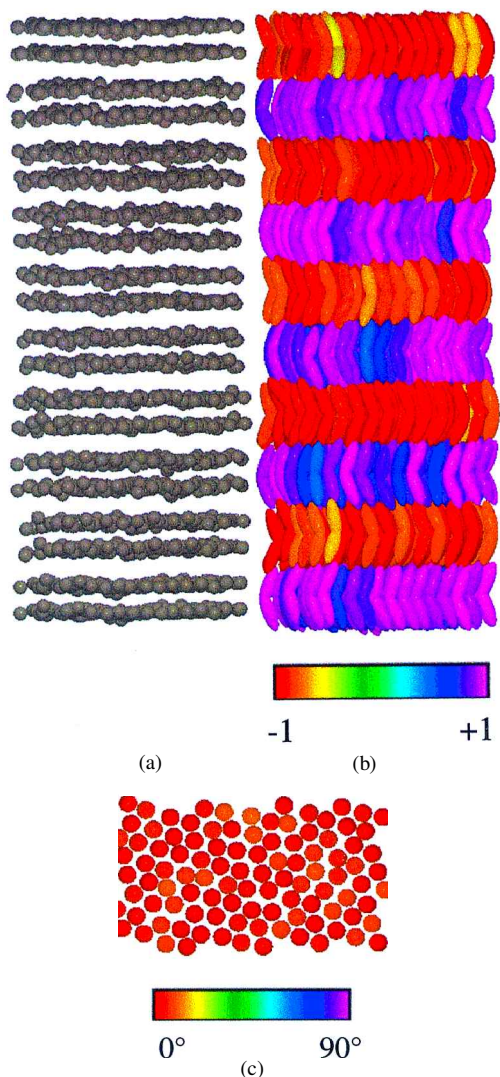
Figure 8. Snapshot of the molecular organization in the layered phase formed at $T^* = 1.5$: (a, b) visualized with vertically aligned layer normal $\hat{\mathbf{l}}$ and horizontally aligned director $\hat{\mathbf{n}}_2$ where each banana-shaped molecule is represented by (a) spheres and (b) ellipsoids for each of its two Gay–Berne centres, in (b) colour-coded according to the projection of the steric dipole $\boldsymbol{\mu}$ on director $\hat{\mathbf{n}}_2$; (c) a selected layer of the system with layer normal $\hat{\mathbf{l}}$ pointing out of the plane where each banana-shaped molecule is represented by a sphere for its molecular centre of gravity colour-coded according to the angle between its molecular long axis x_3^* and the layer normal $\hat{\mathbf{l}}$.

box, ten different layers have been formed, which was enabled by a dramatic elongation of the box side parallel to $\hat{\mathbf{l}}$ as is possible by simulations in the isobaric–isothermal ensemble. Shown in figure 8 (c) is a selected layer of the system with layer normal $\hat{\mathbf{l}}$ pointing out of the plane, where each banana-shaped molecule is represented by a sphere for its molecular centre of gravity. In the phase, there exists no significant tilt angle, and the angle

between the layer normal $\hat{\mathbf{l}}$ and the molecular long axes x_3^* is colour-coded. In the layers each molecule is surrounded by six neighbouring molecules in a preferred hexagonal arrangement. The positional order has been further analysed calculating the bond orientational order parameter for 6-fold order Ψ_6 [28] similarly to a procedure described in [29]. First,

$$\psi_i = \frac{1}{n} \sum_{j=1}^{n} e^{6i\theta_{ij}} \tag{15}$$

is calculated for each molecule i, where θ_{ij} denotes the angle between the vector $\tilde{\mathbf{r}}_{ij}$, defined parallel to the projection of the unit vector $\hat{\mathbf{r}}_{ij}$ between the molecule i and one of its $n = 6$ nearest neighbours j into the plane perpendicular to the layer normal $\hat{\mathbf{l}}$ according to

$$\tilde{\mathbf{r}}_{ij} = \hat{\mathbf{r}}_{ij} - (\hat{\mathbf{r}}_{ij} \ \hat{\mathbf{l}}) \ \hat{\mathbf{l}} \tag{16}$$

and a randomly chosen reference axis perpendicular to the layer normal $\hat{\mathbf{l}}$. Then the bond orientational order parameter Ψ_6 defined as

$$\Psi_6 = \left\langle \frac{1}{N} \sum_{i=1}^{N} |\psi_i| \right\rangle \tag{17}$$

which gives insight into the arrangement of the nearest neighbours, was calculated as the ensemble average expressed by the brackets $\langle \rangle$. The value $\Psi_6 \approx 0.92$ at $T^* = 1.50$, on cooling slightly increasing up to $\Psi_6 \approx 0.93$ at $T^* = 1.25$, indicates that locally the molecules are preferably hexagonally packed.

Of central interest is a detailed investigation of possible polar order in the layered phases, one of the most characteristic features of many smectic phases of banana-shaped molecules, see for example [1, 5]. The long range orientational order of the x_2^* axes has already been proved by significant non-zero order parameters $\langle P_2 \rangle^{(2)}$, which document the preferred parallel orientation of the polar axes x_2^* with respect to the director $\hat{\mathbf{n}}_2$, but give no information about a preferred parallel or antiparallel orientation of the attached steric dipoles $\boldsymbol{\mu}$. Here, detailed insight is obtained considering the longitudinal first rank orientational pair correlation function $S_{110}^{(2,2)}(r_\parallel^*)$, as used, for example, for the characterization of antiphase structures in polar smectic liquid crystals [30], shown in figure 9 as function of the intermolecular separation $r_\parallel^*$ along the layer normal $\hat{\mathbf{l}}$. In the absence of any polar order, the function is zero everywhere. Here, the function is significantly negative for molecules which are separated by short distances along the layer normal; i.e. the steric dipoles of molecules which belong to the same layer are pointing along a common direction, which yields a local layer polarization analysed later. In contrast, the positive sign of $S_{110}^{(2,2)}(r_\parallel^*)$ calculated for molecules separated by
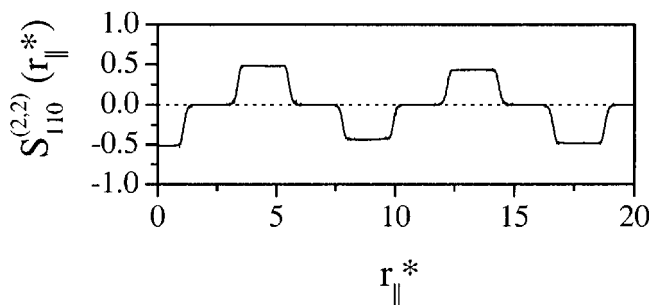
Figure 9. The longitudinal first rank orientational pair correlation function $S_{110}^{(2,2)}(r_{\parallel}^*)$ at temperature $T^* = 1.50$ and its dependence on the intermolecular separation $r_{\parallel}^*$ along the layer normal $\hat{\mathbf{l}}$.

distances of $r_{\parallel}^*$ around the layer distance d_0^* expresses the preferred antiparallel orientation of steric dipoles of molecules belonging to neighbouring layers. This behaviour of $S_{110}^{(2,2)}(r_{\parallel}^*)$ (its sign alternating dependent on $r_{\parallel}^*$), proves an antiferroelectric-like superstructure; i.e. the steric dipoles of molecules separated by an even number of layers and an odd number of layers, respectively, preferably point in the same or the opposite direction, respectively. This antiferroelectric-like superstructure is obvious in the snapshot of the configuration obtained at $T^* = 1.50$ shown in figure 8 (b) where each banana-shaped molecule is represented by ellipsoids for each of its two Gay–Berne centres, colour-coded according to the projection of the steric dipole $\boldsymbol{\mu}$ on director $\hat{\mathbf{n}}_2$. The local polar arrangement of the steric dipoles with an alternating polarization direction moving from layer to layer is obvious. In order to characterize the polar order in more detail and to deduce the presence of ferroelectricity, instead of calculating $\langle P_1 \rangle^{(2)}$ the average global polarization per molecule, $\langle |\mathbf{P}| \rangle = \langle 1/N \, |\Sigma_{i=1}^N \boldsymbol{\mu}_i| \rangle$, has been determined summing up over all N steric dipoles, as for example in a study of the ferroelectric order in nematic liquid crystals [31]. An average global polarization $\langle |\mathbf{P}| \rangle < 0.03$ was determined from a short production run; i.e. $\langle |\mathbf{P}| \rangle$ is essentially zero characterizing an unpolarised system. Additionally, an average local layer polarization per molecule, $\langle |\mathbf{P}_{\text{layer}}| \rangle = \langle 1/m \, \Sigma_{j=1}^m |\mathbf{P}_j| \rangle$, has been calculated where m denotes the number of layers of a configuration and $\mathbf{P}_j$ the polarization per molecule considering molecules arranged in layer j only. A value of $\langle |\mathbf{P}_{\text{layer}}| \rangle \approx 0.94$ clearly shows the existence of local polar order, i.e. a spontaneous local polarization. The antiferroelectric-like superstructure already obvious from the behaviour of $S_{110}^{(2,2)}(r_{\parallel}^*)$ is further proved by calculating average polarizations per molecule, summing separately over the steric dipoles of all molecules of layers with odd and even layer number which have been fixed by reference to a randomly chosen molecule. Values

of

$$\langle |\mathbf{P}_{\text{layer}}^{\text{odd}}| \rangle = \left\langle \frac{1}{N_{\text{odd}}} \left| \sum_{i=1}^{N_{\text{odd}}} \boldsymbol{\mu}_i \right| \right\rangle \approx 0.91$$

and

$$\langle |\mathbf{P}_{\text{layer}}^{\text{even}}| \rangle = \left\langle \frac{1}{N_{\text{even}}} \left| \sum_{i=1}^{N_{\text{even}}} \boldsymbol{\mu}_i \right| \right\rangle \approx 0.89,$$

where N_{odd} and N_{even} denote the number of molecules which belong to layers with odd or even layer number, respectively; i.e. polarizations with similar absolute values, but antiparallel polarization directions $\mathbf{P}_{\text{layer}}^{\text{even}}$ and $\mathbf{P}_{\text{layer}}^{\text{odd}}$ have been obtained. Except for the in-plane positional order the layered phase of achiral banana-shaped Gay–Berne molecules shows all characteristic structural features of the C_{PA}-phase, the antiferroelectric analogue of the C_{P}-phase [32], as recently observed experimentally for the first time for an achiral banana-shaped 4-cyanoresorcinol derivative having an achiral orthogonal biaxial smectic phase exhibiting antiferro-electric switching behaviour [33]. It should be pointed out here that the spontaneous local polarization and the antiparallel polarization of neighbouring smectic layers in the system studied by computer simulation is an effect of both the anisotropy in shape and the attractive interactions of banana-shaped molecules with a steric dipole, but without considering dipole–dipole interactions. Recently, in layered systems of banana-shaped molecules composed of two hard spherocylinders, a considerable biaxial ordering within each layer could also be detected, but no correspondence between the biaxial order in neighbouring layers (i.e. no global phase biaxiality) could be proved [13]. For the coupling between the local polarization of different layers, in addition to steric factors the interactions between the calamitic parts of the banana-shaped molecules (i.e. the molecular end groups) are found to be essential. For the banana-shaped molecules studied with a bending angle of 140°, an antiferroelectric-like superstructure was favoured by the comparable attractive interaction between two molecules of neighbouring layers, if these are preferably arranged with antiparallel steric dipole due to the resulting energetically favourable end-to-end orientation of two calamitic Gay–Berne particles.

One of the most interesting features recently discovered in liquid crystal phases of achiral banana-shaped molecules is the formation of chiral domains, i.e. spontaneous achiral symmetry breaking [3–8]. Many possible structures are still under discussion for these chiral domains, which seem to be connected to the existence of long range positional order in the form of the layers, as for example in the model of Link et al. [5] where each layer itself is chiral due to a combination of two symmetry breaking

directions, the local layer polarization and the tilt. As shown above, there exists a local layer polarization in the layers formed at $T^* = 1.50$, but due to the absence of any tilt these layers are achiral. Recently, a further possibility for helical superstructures in phases of achiral banana-shaped molecules has been suggested, considering a splitting in right-handed and left-handed domains with a so-called twist–bend structure [34] as sketched in figure 10(a). In such a domain, the local director $\hat{\mathbf{n}}(z)$ is considered spiralling around the helical axis according to equation (5), with constant tilt angle θ and pitch P defining the helical periodicity leading to a z-dependent azimuthal angle, see figure 10(b), i.e. the director field corresponds to the well known situation in a chiral smectic C* phase, figure 10(c), and to a model theoretically considered for cholesteric phases with conic structures [35].

In the following, such structures will be considered for the nematic-like phase close to the phase transition to the smectic, where it still lacks an explanation for the already mentioned low order parameters $\langle P_2 \rangle^{(3)}$ (figure 5). A deeper insight into its peculiar structural properties is obtained by inspection of the snapshot shown in figure 11, where a configuration chosen at $T^* = 1.75$ from the cooling sequence which yielded structures with comparable low order parameter $\langle P_2 \rangle^{(3)}$, has been visualized with a vertically aligned space-fixed director $\hat{\mathbf{n}}_3$ found to be constrained parallel to z. Obviously, no layers have been formed, figure 11(a). The comparable low global order parameter seems to be due to a super-structure, figure 11(b), which apparently shows similarities to the twist–bend structure discussed above as a possible structure in chiral domains of banana-shaped molecules, figure 10(a).
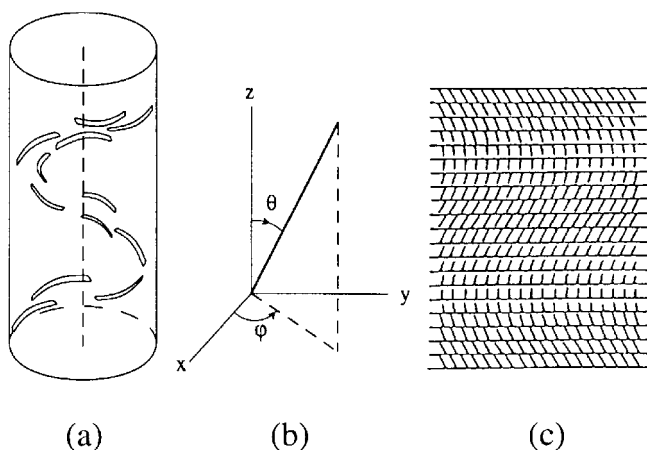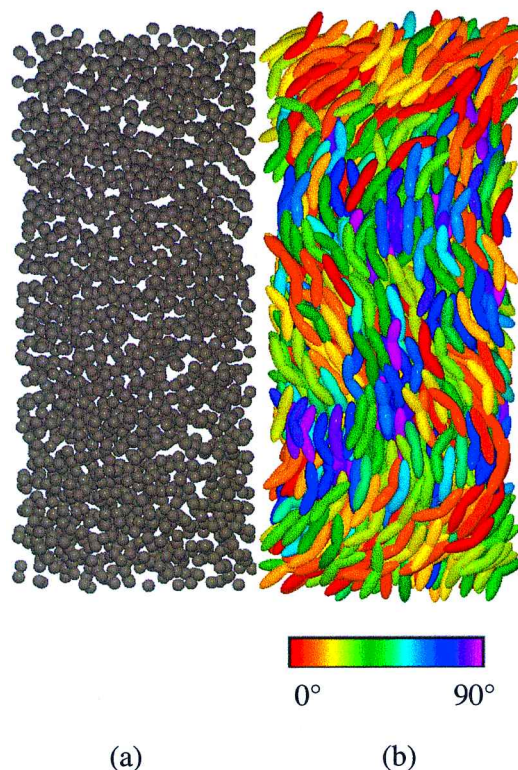

$0°$ $90°$

(a)   (b)

Figure 11. Snapshot of the molecular organization in the phase formed at $T^* = 1.75$ visualized with a vertically aligned director $\hat{\mathbf{n}}_3$ where each banana-shaped molecule is represented by (a) spheres and (b) ellipsoids for each of its two Gay–Berne centres, in (b) colour-coded according to the azimuthal angle of the molecular long axis x_3^*.

In order to demonstrate the existence of such a helical superstructure, the longitudinal correlation function $S_{220}^{(3,3)}(r_{\parallel}^*)$ has been calculated as a function of the inter-molecular separation $r_{\parallel}^*$ along the director $\hat{\mathbf{n}}_3$ and the z-axis, respectively (figure 12). Apart from short range effects, in a nematic phase $S_{220}^{(3,3)}(r_{\parallel}^*)$ is independent of the intermolecular separation $r_{\parallel}^*$ along the director. In contrast, in a cholesteric phase $S_{220}^{(3,3)}(r_{\parallel}^*)$ is modulated

Figure 10. Twist–bend structures: (a) a right-handed domain of banana-shaped molecules; (b) spiralling tilted local director $\hat{\mathbf{n}}(z)$, see equation (5); (c) director configuration of a chiral smectic C* phase (figures from [34]).
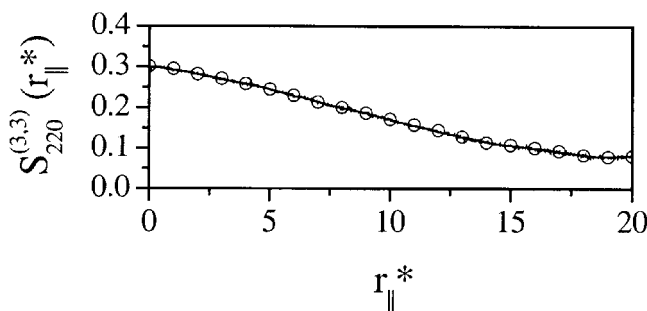

Figure 12. The longitudinal second rank orientational pair correlation function $S_{220}^{(3)}(r_{\parallel}^*)$ at temperature $T^* = 1.75$ and its dependence on the separation $r_{\parallel}^*$: (a) along the space-fixed director $\hat{\mathbf{n}}_3$ (——); (b) along the space-fixed z-axis (○).

dependent on the intermolecular separation $r_{\parallel}^*$ along the helical axis due to the spiralling superstructure, see for example [36]. It varies monotonously from a positive maximum for molecules separated by small values of $r_{\parallel}^*$ (locally the molecules are preferably parallel to each other), to a negative minimum at distance $r_{\parallel}^* = P^*/4$, where P^* denotes the scaled pitch defining the periodicity; i.e. molecules separated by this distance along the helical axis are preferably perpendicular to each other. In the phase of the banana-shaped molecules observed at $T^* = 1.75$, $S_{220}^{(3,3)}(r_{\parallel}^*)$ shows a similar behaviour calculated along the director $\hat{\mathbf{n}}_3$. The positive minimum value can be understood considering a helical superstructure with a tilted local director, where for no distance along the helical axis preferred local orientations perpendicular to each other exist. The helical axis is found to be along the z-axis, an effect related to the periodic boundaries conditions applied as discussed in detail in, for example, [36], which is obvious due to the superimposing curves shown in figure 12.

An additional local order parameter $\langle \tilde{P}_2 \rangle^{(3)}$ of the molecular long axis x_3^* has been calculated with respect to a spiralling tilted local director $\hat{\mathbf{n}}(z)$ as described in §4. The helical axis was taken to be constrained along the z-axis, considering that one segment with a length of the pitch has been formed inside the simulation box, i.e. pitch $P^* = L_z^*$. Shown in figure 13 is the evolution of selected structural quantities during the production run at $T^* = 1.75$. If calculated with respect to a tilted local director $\hat{\mathbf{n}}(z)$ spiralling with the appropriate handedness, here right-handed, the local order parameter $\langle \tilde{P}_2 \rangle^{(3)}$ (see also figure 5) is significantly larger compared with the comparable small global order parameter $\langle P_2 \rangle^{(3)}$, a behaviour obvious over the complete production run of 200 000 cycles, figure 13 (a). An average tilt angle $\theta \approx 20.5°$ and a scaled pitch $P^* \approx 41.7$ have been determined averaging over the production run, figure 13 (b).

In order to prove the helical superstructure in more detail, an appropriate pseudoscalar correlation function, $S_{221}^{(3,3)}(r_{\parallel}/P)$, has been determined as a function of the intermolecular separation $r_{\parallel}^*$ scaled by pitch P along the z-axis. In a phase without a helical superstructure, e.g. a nematic phase where right- and left-handed molecular arrangements have the same probability, this function would be zero independent of the separation along the selected reference axis. In contrast, $S_{221}^{(3,3)}(r_{\parallel}/P)$ given in figure 14 shows the characteristic behaviour of phases with helical superstructures, see for example [20] for its behaviour in blue or cholesteric phases. It has small, but significantly non-zero values and the minimum corresponds to a separation of $P/4$ along the helical axis. The negative values characterize a right-handed helical structure, a feature obvious over the complete production run considering separately configurations taken from
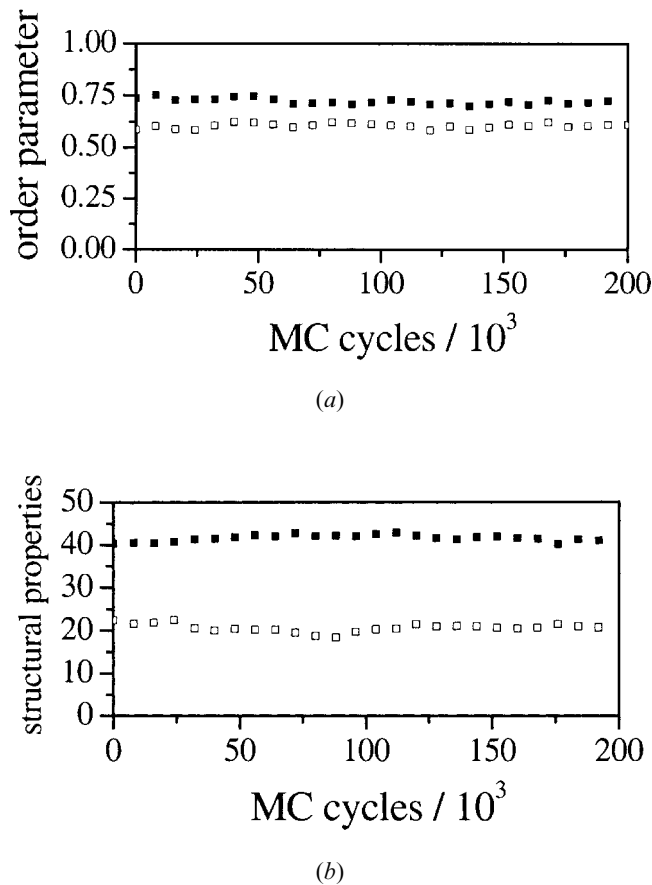
(a)

(b)

Figure 13. Evolution of structural properties during the production run at $T^* = 1.75$: (a) global order parameter $\langle P_2 \rangle^{(3)}$ calculated with respect to a space-fixed director $\hat{\mathbf{n}}_3$ (□) and local order parameter $\langle \tilde{P}_2 \rangle^{(3)}$ calculated with respect to a right-handed spiralling tilted local director $\hat{\mathbf{n}}(z)$ (■); (b) tilt angle θ (□) and scaled pitch P^* (■).
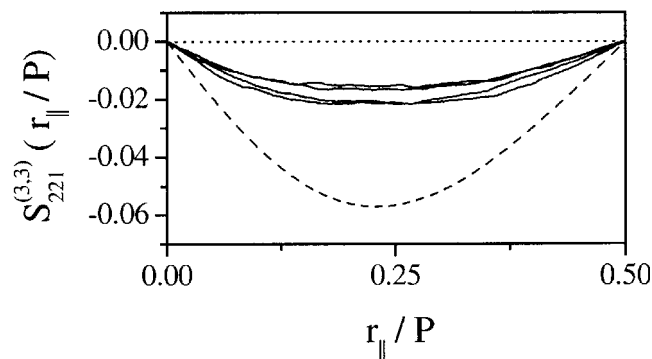
Figure 14. The pseudoscalar longitudinal second rank orientational pair correlation function $S_{221}^{(3,3)}(r_{\parallel}/P)$ at temperature $T^* = 1.75$ calculated along the helical axis parallel to z (—, from 1000 configurations selected after blocks of 50 000 cycles each). For comparison, additionally shown are the corresponding functions in a nematic phase (⋯) with perfect order, i.e. $\langle P_2 \rangle^{(3)} = 1$, and in a helical phase (---) with a right-handed spiralling tilted local director $\hat{\mathbf{n}}(z)$, and tilt angle $\theta = 20°$ and perfect local order $\langle \tilde{P}_2 \rangle^{(3)} = 1$.

selected parts of the production run. In systems composed of achiral molecules only the corresponding left-handed structure should appear with equal probability, but they could be separated by large free enthalpy barriers. Further investigations are necessary in order to clarify whether the right-handed domain formed (which due to the small system size studied, corresponds to the whole system) represents a metastable state only; i.e. whether a global free enthalpy minimum exists for a stable untwisted state which again could be separated by large free enthalpy barriers. The results of a second cooling sequence give a first hint for such a behaviour. Again a nematic phase has been formed, now even close to the second phase transition without helical super-structure and significantly enlarged global order parameter $\langle P_2 \rangle^{(3)}$ (figure 5), but with thermodynamic properties $\langle V^* \rangle$ and $\langle H^* \rangle$ (figure 3) in good agreement; i.e. both the achiral and the chiral structure could be of similar free enthalpy. Under periodic boundary conditions the formation of a helical superstructure is enabled for selected orientations of the helical axis only, as discussed in detail in [36], e.g. parallel to a box face normal; whereas in the second cooling sequence nematic phases with a director $\hat{\mathbf{n}}_3$ oriented oblique to a box face normal have been formed, a state necessarily separated by large free enthalpy barriers from a chiral state, as observed previously.

In fact, the spontaneous achiral symmetry breaking in nematic phases composed of achiral banana-shaped molecules observed in the simulation has been recently discussed based on the speculation that in such phases the bend elastic constant K_3 could be negative [37]. Under this hypothesis, a simple Landau-like model predicts a second order phase transition inside the nematic phase, from uniform to spatially modulated director, either oscillating splay–bend or uniform conical twist–bend with twofold degenerated left- or right-handed twist, the latter corresponding to the helical superstructure formed in the simulation.

6. Conclusions

Molecular systems of achiral banana-shaped molecules have been studied by means of Monte Carlo simulations in the *NpT* ensemble, taking into account both translational and orientational degrees of freedom, in order to determine relationships between molecular structure and phase properties. The systems were composed of rigid, biaxial molecules of point symmetry group C_{2v}, characterized by a suitable bending angle $\varphi = 140°$ and a steric dipole, with interactions described by the Gay–Berne potential. A rich polymorphism of liquid crystal phases, proven by order parameters, scalar and pseudo-scalar orientational correlation functions, and visual representations of selected configurations, was observed

dependent upon temperature. For the first time by computer simulation of many-particle systems of banana-shaped molecules, an untilted smectic phase with global phase biaxiality and a local polar arrangement of the steric dipoles with an antiferroelectric-like superstructure has been formed at low temperature, a phase structure which recently has been discovered experimentally [33]. The clear evidence should be emphasised that the spontaneous local polarization and the antiparallel polarization of neighbouring smectic layers are due to the anisotropy in shape and attractive interactions of the banana-shaped molecules with a steric dipole only, without considering dipole–dipole interactions. Remarkable is the formation of nematic phases at intermediate temperature, a feature which has been observed in systems of banana-shaped molecules only in exceptional cases [24, 25]. In the nematic phase, close to the phase transition to the highly ordered smectic phase, even hints of a spontaneous achiral symmetry breaking have been determined by means of a pseudoscalar orientational correlation function and an analysis of the local order with respect to a tilted, continuously spiralling reference system. The helical superstructure observed could correspond to the uniform conical twist–bend structure existing with twofold degenerated left- or right-handed twist, as recently predicted for achiral banana-shaped molecules by considering the effects of a negative bend elastic constant with respect to the formation of nematic phases with spatially modulated director by means of a simple Landau-like model [37]. With respect to the appearance of spontaneous achiral symmetry breaking in the phase without smectic layers, further investigations are necessary, especially taking into account larger system sizes and longer simulation runs, in order to clarify whether the chiral domain formed in the simulation corresponds to a stable or metastable state (i.e. a global free enthalpy minimum exists for a stable untwisted state), or whether it appeared due to fluctuations only. Further challenging tasks are extended studies taking into account internal degrees of freedom, of interest with respect to the significance of chiral conformers of achiral banana-shaped molecules [4], and consideration of the effect of external fields, especially the switching behaviour of phases with antiferroelectric-like superstructure.

References

[1] NIORI, T., SEKINE, T., WATANABE, J., FURUKAWA, T., and TAKEZOE, H., 1996, *J. mater. Chem.*, **6**, 1231.

[2] BLINOV, L. M., 1998, *Liq. Cryst.*, **24**, 143.

[3] *Banana-shaped liquid crystals: Chirality by achiral molecules*, Workshop, Technical University of Berlin, Sfb 335 'Anisotrope Fluide', 1997.

[4] SEKINE, T., NIORI, T., SONE, M., WATANABE, J., CHOI, S.-W., TAKANISHI, Y., and TAKEZOE, H., 1997, *Jpn. J. appl. Phys.*, **36**, 6455.

[5] LINK, D. R., NATALE, G., SHAO, R., MACLENNAN, J. E., CLARK, N. A., KÖRBLOVA, E., and WALBA, D. M., 1997, *Science*, **278**, 1924.

[6] HEPPKE, G., and MORO, D., 1998, *Science*, **279**, 1872.

[7] WATANABE, J., NIORI, T., SEKINE, T., and TAKEZOE, H., 1998, *Jpn. J. appl. Phys.*, **37**, L139.

[8] JÀKLI, A., LISCHKA, C., WEISSFLOG, W., PELZL, G., and SAUPE, A., 2000, *Liq. Cryst.*, **27**, 1405.

[9] PASINI, P., and ZANNONI, C. (editors), 1999, *Advances in the Computer Simulations of Liquid Crystals* (Dordrecht: Kluwer Academic Publishers).

[10] CRAIN, J., and KOMOLKIN, A. V., 1999, *Advances in Chemical Physics*, Vol. 109, edited by I. Prigogine and S. A. Rice (Chichester: John Wiley), p. 39.

[11] MEMMER, R., KUBALL, H.-G., and SCHÖNHOFER, A., 1996, *Mol. Phys.*, **89**, 1633.

[12] NEAL, M. P., PARKER, A. J., and CARE, C. M., 1997, *Mol. Phys.*, **91**, 603.

[13] CAMP, P. J., ALLEN, M. P., and MASTERS, A. J., 1999, *J. chem. Phys.*, **111**, 9871.

[14] BILLETER J. L., and PELCOVITS, R. A., 2000, *Liq. Cryst.*, **27**, 1151.

[15] DIELE, S., PELZL, G., and WEISSFLOG, W., 1999, *Liq, Cryst. Today*, **9**, 8.

[16] PELZL, G., DIELE, S., GRANDE, S., JÀKLI, A., LISCHKA, CH., KRESSE, H., SCHMALFUSS, H., WIRTH, I., and WEISSFLOG, W., 1999, *Liq. Cryst.*, **26**, 401.

[17] GAY, J. G., and BERNE, B. J., 1981, *J. chem. Phys.*, **74**, 3316.

[18] BATES, M. A., and LUCKHURST, G. R., 1999, *Liquid Crystals I*, edited by D. M. P. Mingos (Berlin: Springer), p. 65.

[19] FRENKEL, D., and SMIT, B., 1996, *Understanding Molecular Simulation* (San Diego: Academic Press).

[20] MEMMER, R., 2001, *J. chem. Phys.*, **114**, 8210.

[21] STONE, A. J., 1978, *Mol. Phys.*, **36**, 241.

[22] HASHIM, R., LUCKHURST, G. R., and ROMANO, S., 1995, *J. chem. Soc., Faraday Trans.*, **91**, 2141.

[23] BATES, M. A., and LUCKHURST, G. R., 1999, *J. chem. Phys.*, **110**, 7087.

[24] SHEN D., DIELE, S., PELZL, G., WIRTH, I., and TSCHIERSKE, C., 1999, *J. mater. Chem.*, **9**, 661.

[25] MATRASZEK, J., MIECZKOWSKI, J., SZYDŁOWSKA, J., and GÒRECKA, E., 2000, *Liq. Cryst.*, **27**, 429.

[26] ZANNONI, C., 2001, *Physical Properties of Liquid Crystals*, edited by D. A. Dunmur, A. Fukuda, and G. R. Luckhurst (London: IEE), p. 624.

[27] WITHERS, I. M., CARE, C. M., and CLEAVER, D. J., 2000, *J. chem. Phys.*, **113**, 5078.

[28] STRANDBURG, K. J. (editor), 1992, *Bond-Orientational Order in Condensed Matter Systems* (New York: Springer).

[29] BILLETER, J., and PELCOVITS, R., 1998, *Comput. Phys.*, **12**, 440.

[30] BERARDI, R., ORLANDI, S., and ZANNONI, C., 1996, *Chem. Phys. Lett.*, **261**, 357.

[31] AYTON, G., and PATEY, G. N., 1996, *Phys. Rev. Lett.*, **76**, 239.

[32] BRAND, H. R., CLADIS, P. E., and PLEINER, H., 1992, *Macromolecules*, **25**, 7223.

[33] EREMIN, A., DIELE, S., PELZL, G., NÀDASI, H., WEISSFLOG, W., SALFETNIKOVA, J., and KRESSE, H., 2001, in Proceedings of the 6th European Conference on Liquid Crystals. 25–30 March, 2001, Halle, Germany, 4–P4.

[34] LAGERWALL, S. T., 1999, *Ferroelectric and Anti-ferroelectric Liquid Crystals* (Weinheim: Wiley-VCH).

[35] PLEINER, H., and BRAND, H. R., 1993, *J. Phys. II Fr.*, **3**, 1397.

[36] MEMMER, R., 2000, *Liq. Cryst.*, **27**, 533.

[37] DOZOV, I., 2001, in Proceedings of the 6th European Conference on Liquid Crystals. 25–30 March, 2001, Halle, Germany, 8–P09.